POLITECNICO
MILANO 1863

SCUOLA DI INGEGNERIA INDUSTRIALE
E DELL'INFORMAZIONE

Executive Summary of the Thesis

A sensitivity analysis of laser-propelled sail trajectories for a mission to Proxima Centauri

Laurea Magistrale in Space Engineering - Ingegneria Spaziale

Author: Federico Infantino

Advisor: Prof. Camilla Colombo

Co-advisor:

Academic year: 2022-2023

1. Introduction

This document is the executive summary the master's thesis, titled 'A sensitivity analysis of laser-propelled sail trajectories for a mission to Proxima Centauri'. The thesis develops a numerical model for propagating the trajectory of a highly reflective, super-light sail headed towards Proxima Centauri. This model integrates a relativistic three-body problem with laser acceleration models within the Solar System, and the Galactic potential model beyond the Solar System's Hill sphere. The primary research objective is to analyze the sensitivity of the optimal beam orientation (laser acceleration) necessary to reach the target, considering all perturbations in the model. This included assessing random errors during the acceleration phase and their overall impact on the trajectory, to analyze the sensitivity of the solution. This summary concisely reports the overarching objectives, methodologies employed, and the key results and impacts of the research.

2. Methodology

The method used in this research is a numerical propagation of the trajectory. Using an ODE solver with given initial conditions, an optimal solution is found in terms of right ascension α_{opt} and declination δ_{opt} of the vector describing the orientation of the laser beam in an Sun-centred equatorial frame. The optimization process finds the optimal direction of acceleration to minimize the distance from Proxima Centauri at arrival. The mission consists of a Solar System escape phase and a Galactic phase. The models involved in the simulation are reported in the following sections.

2.1. Laser acceleration model

The laser propulsion is modelled according to the relativistic solution for the acceleration, given by Kulkarni et al. [4]:

$$\begin{cases} \dfrac{2P}{mc^2\gamma^3}\dfrac{(1-\beta)}{(1+\beta)}, & x \leq L_0 \\ \dfrac{2P}{mc^2\gamma^3}\dfrac{(1-\beta)}{(1+\beta)}\left(\dfrac{L_0}{x}\right)^2, & x > L_0 \end{cases} \tag{1}$$

where $\beta = v/c$ is the ratio of the spacecraft's velocity and the speed of light, P is the laser power, m is the total mass of the spacecraft and γ is the Lorentz factor that takes into account relativistic effects. Equation 1 shows the analytical expression of the acceleration due to

an incident laser beam on the sail, considering diffraction of light beyond the critical point L_0, where the laser spot size is equal to the size of the sail. The involved masses, boost times and sail parameters are described in detail in the main work as well as the original paper by Lubin [5].

2.2. Relativistic three-body problem

While the laser propulsion is active, the spacecraft reaches relativistic speeds while being under the influence of Earth's gravity, beginning its trajectory from a parking orbit around Earth. Upon exiting Earth's sphere of influence, the Sun's gravitational acceleration also comes into play. This phase is modeled as a relativistic three-body problem, applying the solution to the Relativistic N-body Problem as provided by Masat [6], leading to the following equations:

$$\begin{aligned}\mathbf{a}_{\mathrm{Rel},sc} = & -\frac{\mu_E}{|\mathbf{d}|^3}\mathbf{d}\left\{-\frac{4\mu_{sun}}{c^2|\mathbf{r}|}-\frac{\mu_{sun}}{c^2|\boldsymbol{\rho}|}+\left(\frac{|\dot{\mathbf{r}}|}{c}\right)^2+\right.\\ & \left.+2\left(\frac{|\dot{\boldsymbol{\rho}}|}{c}\right)^2-\frac{4(\dot{\mathbf{r}}\cdot\dot{\boldsymbol{\rho}})}{c^2}-\frac{3\left[\frac{\mathbf{d}\cdot\dot{\boldsymbol{\rho}}}{|\mathbf{d}|}\right]^2}{2c^2}\right\}+\\ & -\frac{\mu_{sun}}{|\mathbf{r}|^3}\mathbf{r}\left\{-\frac{4\mu_E}{c^2|\mathbf{d}|}-\frac{\mu_E}{c^2|\boldsymbol{\rho}|}+\left(\frac{|\dot{\mathbf{r}}|}{c}\right)^2\right\}+\\ & +\frac{\mu_E}{c^2|\mathbf{d}|^3}\left\{\mathbf{d}\cdot[4\dot{\mathbf{r}}-3\dot{\boldsymbol{\rho}}]\right\}\dot{\mathbf{d}}+\\ & +\frac{\mu_{sun}}{c^2|\mathbf{r}|^3}\left\{\mathbf{r}\cdot 4\dot{\mathbf{r}}\right\}\dot{\mathbf{r}}+\\ & +\frac{\mu_{\mathrm{E}}}{2c^2|\mathbf{d}|^3}(-\mathbf{d})(-\mathbf{d})\cdot\ddot{\boldsymbol{\rho}}+\frac{7\mu_{\mathrm{E}}\ddot{\boldsymbol{\rho}}}{2c^2|\mathbf{d}|}\end{aligned}$$

Where $\mathbf{r}$ and $\mathbf{d}$ represent the spacecraft's position vectors relative to the Sun and Earth, respectively, while $\boldsymbol{\rho}$ denotes Earth's position relative to the Sun. μ_E and μ_{Sun} are the gravitational parameters of Earth and the Sun respectively, $\dot{\mathbf{r}}$ and $\mathbf{r}$ represent velocity and position of the spacecraft in a heliocentric frame, and c is the speed of light. As the spacecraft traverses the Hill sphere of the Solar System, defined in Souami (2020) [7], the gravitational influence of the Solar System, specifically that of the Sun and Earth, can be considered no longer dominant in this approach. Consequently, the spacecraft becomes subject to the gravitational forces of the Galaxy. This transition is modeled using the Galactic potential model as described by Irrgang (2013) [2], and the equations of motion outlined by Dybczyński (2015) [1]:

$$\begin{aligned}\ddot{x} = & G\left(-\frac{x\cdot M_b}{(R^2+b_b^2)^{3/2}}-\frac{x\cdot M_d}{(x^2+y^2+(a_d+\sqrt{z^2+b_d^2})^2)^{3/2}}+\right.\\ & \left.-\frac{x\cdot M_h}{a_h\cdot R\cdot(a_h+R)}\right)\\ \ddot{y} = & G\left(-\frac{y\cdot M_b}{(R^2+b_b^2)^{3/2}}-\frac{y\cdot M_d}{(x^2+y^2+(a_d+\sqrt{z^2+b_d^2})^2)^{3/2}}+\right.\\ & \left.-\frac{y\cdot M_h}{a_h\cdot R\cdot(a_h+R)}\right)\\ \ddot{z} = & G\left(-\frac{z\cdot M_b}{(R^2+b_b^2)^{3/2}}+\right.\\ & -\frac{z\cdot M_d\left(a_d+\sqrt{z^2+b_d^2}\right)}{\left(\sqrt{z^2+b_d^2}\right)\left(x^2+y^2+(a_d+\sqrt{z^2+b_d^2})^2\right)^{3/2}}+\\ & \left.-\frac{z\cdot M_h}{a_h\cdot R\cdot(a_h+R)}\right)\end{aligned}$$

In the equations above, the accelerations along x y and z in a Galactocentric frame are reported, while $M_b, M_d, M_h, b_b, a_h, a_d$ are constants related to the bulge, disk and halo components of the Galaxy, reported in the paper mentioned before, as well as the Galactocentric spherical radius R defined as:

$$R = \sqrt{r^2+z^2} \tag{2}$$

where

$$r = \sqrt{x^2+y^2} \tag{3}$$

where x, y and z are Galactocentric coordinates.

3. Trajectory propagation

3.1. Optimal solution

An optimal solution is identified through the minimization of the arrival distance, considering all model perturbations. The result is a unit vector that specifies the optimal direction of acceleration for the particular mission scenario under consideration. This vector is calculated in an equatorial frame using the α_{opt} and δ_{opt} coordinates. The subsequent step involves assessing the sensitivity of this optimal solution to random Gaussian-distributed errors during the pointing phase. This analysis aims to understand their impact on the trajectory and to establish a maximum threshold for pointing errors, in connection to the success of the mission.

3.2. Sensitivity analysis

The sensitivity of the optimal solution is then tested considering the following sources of errors:

- Pointing errors in the acceleration laser beam
- Position errors in the parking orbit with respect to a nominal $\mathbf{r_0}$ position vector.
- Boost time errors

with the following standard deviations:

Variable nominal value	Standard deviations σ
$\alpha_{optimal}$	0.01 - 1 [deg]
$\delta_{optimal}$	0.01 - 1 [deg]
$\text{time}_{propulsion}$	0.01 - 1 [s]
Initial position vector orientation	0.01 - 1 [deg]

Table 1: The column of the standard deviations shows a range of standard deviations used to propagate the trajectories. The assumed values do not reflect real standard deviations in a real mission scenario but are arbitrary values.

A swarm of 1000 spacecraft, each with a unique set of initial conditions influenced by errors, is initialized. The outcomes are presented here, focusing on three scenarios for the case where m_{sail} equals 1 gram and the achieved speed is $v = 0.2$ c:

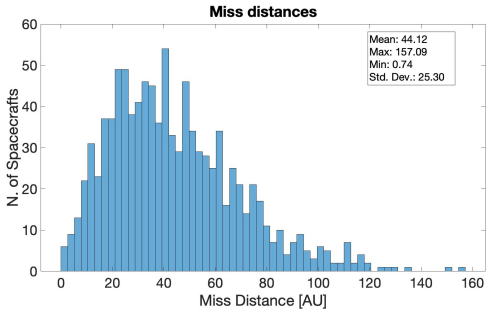

Figure 1: Miss distances from Proxima Centauri with 1000 launches with a **0.01 degrees** standard deviation for the pointing and initial position and **0.01 seconds** for the boost time. It's important to note that the exact output values may differ from the original work, as the outcomes are random according to the random errors in the simulations.

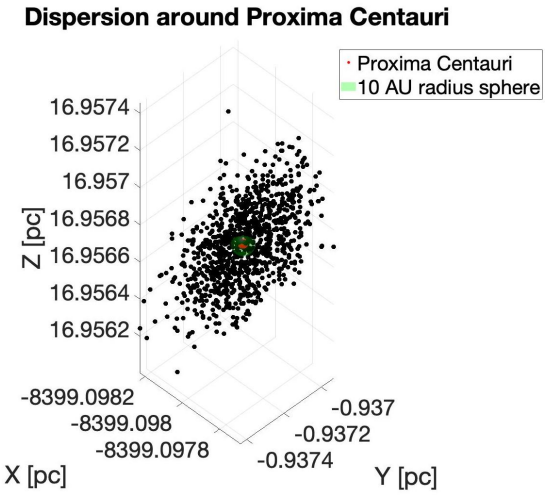

Figure 2: Dispersion plot around Proxima Centauri in a galactocentric reference frame. Proxima Centauri (i.e. the centre of its volume error) is not in scale.

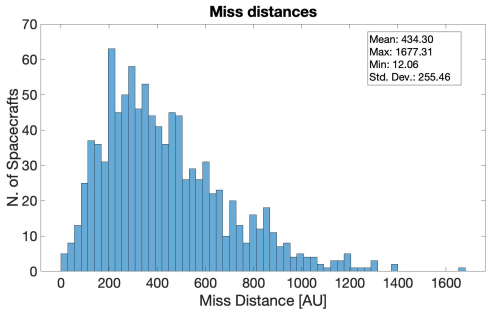

Figure 3: Miss distances from Proxima Centauri with 1000 launches with a **0.1 degrees** standard deviation for the pointing and initial position and **0.1 seconds** for the boost time.

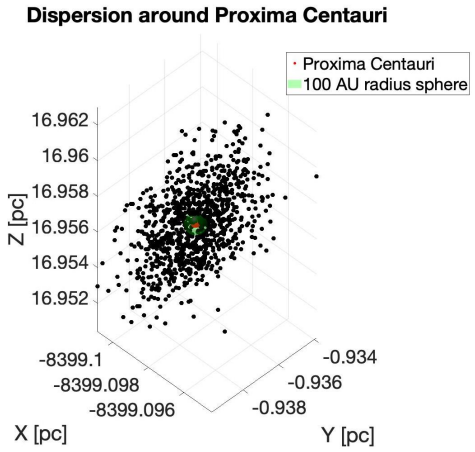

Figure 4: Dispersion plot around Proxima Centauri. The reference sphere here is 100 AU. Proxima Centauri is not in scale.

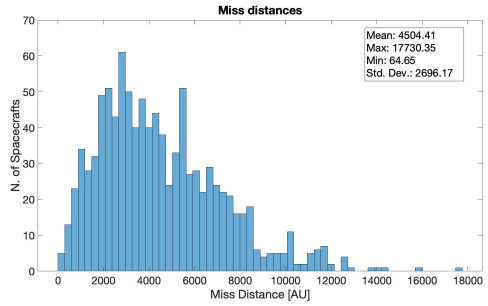

Figure 5: Miss distances from Proxima Centauri with 1000 launches with a **1 degrees** standard deviation for the pointing and initial position and **1 seconds** for the boost time.

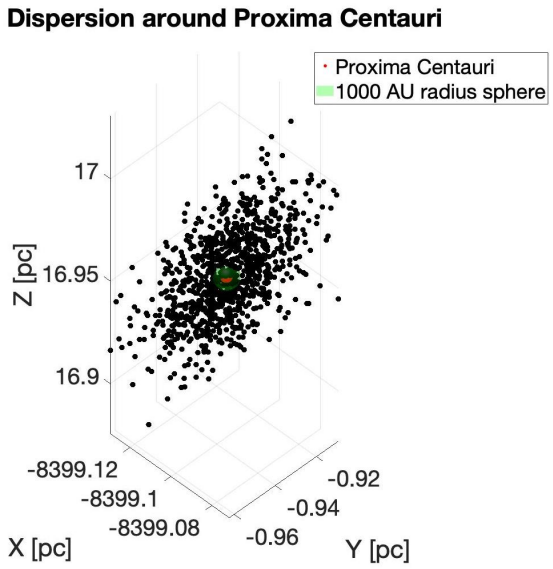

Figure 6: Dispersion plot around Proxima Centauri. The reference sphere here is 1000 AU. Proxima Centauri is not in scale.

The results indicate that with each order of magnitude increase in standard deviations, the mean error correspondingly increases, mirroring the findings of A. Jackson [3]. The analysis also reveals that pointing errors are the primary contributors to trajectory deviations, while errors in boost times and initial orientation result in deviations of approximately 10^{-3} AU. The magnitudes of errors obtained and shown in the previous histograms exceed the spacecraft's capacity for trajectory correction, highlighting the critical importance of pointing accuracy during the acceleration phase.
Lubin [5] suggests that trajectory adjustments up to 1 AU might be achievable, utilizing the electrical and thermal components of thrust from an onboard RTG (Radioisotope Thermoelectric Generator) with 0.3 grams of Pu-238 over an estimated 20-year mission. However, given the simplifications in the model and potential future improvements in trajectory correction technology, a conservative margin is considered. Consequently, the safe zone is defined as being within less than 3 AU from the target.
Setting this threshold to define mission success and focusing solely on pointing errors, the following is observed:

σ_{pointing} [arcsec]	**Mean Success Rate** (Miss distance $<$ 3 AU)
36	0.53%
28.8	0.67%
21.6	1.07%
18	1.53%
10.8	4.33%
7.2	9.77%
3.6	35.04%
2.88	47.15 %
2.16	64.9 %
1.8	74.5 %
1.08	95.71 %
0.72	99.4 %
0.36	100 %

Table 2: Mean success rates for various standard deviations of the pointing errors. The success rate is defined as the fraction of spacecrafts that intercepts the target with a miss distance smaller than 3 AU. The simulations are performed for 1000 launches.

Table 2 illustrates that the precision needed for this model to reach the target within a 3 AU distance is approximately ~ 1 arcsecond or less. The scenario with $\sigma_{pointing} = 36$ arcseconds or 0.01 degrees, also depicted in Figure 1, results in a mean success rate of 0.53% across 1000 launches. A 100% mean success rate is achieved with a pointing standard deviation of $\sigma_{pointing} = 0.36$ arcseconds or 10^{-4} degrees. Furthermore, a 96.7% success rate is observed when assuming a miss distance of 1 AU from the target.

4. Conclusions

The study simulates interstellar travel using a laser-propelled spacecraft, revealing the critical

impact of pointing inaccuracies on the mission's success. Even arcsecond-level errors can cause significant deviations, with a pointing accuracy range of 0.01 to 1 degrees leading to off-target distances of tens of thousands of AU. Pointing errors are dominant with respect to the considered errors due to the boosting times and to the initial orientation of the spacecraft on the parking orbit. However, maintaining standard deviations within 0.36 arcseconds ensures a 100% success rate, assuming it as the spacecraft's arrival within 3 AU of Proxima Centauri. The findings emphasize the trajectory's sensitivity to initial conditions, revealing the need of a high precision lasers with precision pointing in the order of $\sim$ 1 arcsecond or even less, threshold that may change according to the definition of the considered mission success.

References

[1] Piotr A. Dybczyń ski and Filip Berski. On the accuracy of close stellar approaches determination. *Monthly Notices of the Royal Astronomical Society*, 449(3):2459–2471, apr 2015.

[2] A. Irrgang, B. Wilcox, E. Tucker, and L. Schiefelbein. Milky way mass models for orbit calculations. *Astronomy & Astrophysics*, 549:A137, Jan 2013. Number of page(s): 13, Section: Galactic structure, stellar clusters and populations, Published online: 15 January 2013.

[3] A Jackson. Dispersion analysis of small-scale-spacecraft interstellar trajectories. 2017.

[4] Neeraj Kulkarni, Philip Lubin, and Qicheng Zhang. Relativistic spacecraft propelled by directed energy. *The American Astronomical Society*, 155(4), 2018.

[5] Philip Lubin. A roadmap to interstellar flight. *JBIS*, 69:40–72, 2016.

[6] Alessandro Masat. B-plane orbital resonance analysis and applications. perturbed semi-analytical model for planetary protection and defence applied to ballistic resonant flyby design. Master's thesis, Politecnico di Milano, Milano, 2019. URL = `https://hdl.handle.net/10589/151660`.

[7] Damya Souami, Jacky Cresson, Christophe Biernacki, and Frédéric Pierret. On the local and global properties of gravitational spheres of influence. *Monthly Notices of the Royal Astronomical Society*, 496(4):4287–4297, 2020.